

The Effect of Length and Diameter on the Signal-to-Noise Ratio of Evanescent Field Absorption Fiber-Optic Sensors

T. B. COLIN,* K.-H. YANG,*† M. A. ARNOLD, GARY W. SMALL,‡ and W. C. STWALLEY*§

Department of Chemistry, University of Iowa, Iowa City, Iowa 52242

This paper discusses the theoretical and experimental implications of changing the length and diameter of the evanescent field sensing region of an evanescent field sensor. Particular emphasis is placed on optimizing the intensity of the evanescent field for near-infrared sensor applications. Both theoretical and experimental results show that an optimal length and diameter must be determined experimentally for each analyte system.

Index Headings: Infrared; Instrumentation, sensors; Optics; Fiber optics.

INTRODUCTION

Evanescent field fiber-optic sensors have become increasingly popular for remote sensing applications. General spectroscopic systems for mid-IR¹ and near-IR,² as well as specific biosensors³ and distributed sensor systems,⁴ have been developed on the basis of the evanescent field sampling technique. Since the evanescent field intensity is very weak in comparison to the light intensity used in conventional optical techniques, it is important to optimize the evanescent field sensor to gain full advantage of its sensitivity. The focus of this paper is on the optimization of these sensors by adjustment of the length and diameter of the evanescent field sensing region.

THEORY

Light propagation in step index multimode optical fibers can be described in terms of a cylindrical dielectric waveguide which has been described in detail by Snitzer.⁵ The results of these calculations reveal that many modes of propagation are possible, each having a characteristic distribution of intensity between the core and cladding of the optical fiber.

To understand the nature of the evanescent field in a multimode fiber, it is necessary to calculate how much light is propagated by each mode, and how much of the energy of each mode is propagating in the cladding, or *evanescent field*. The modes of interest in fiber-optic sensor development are the HE, EH, TE, and TM modes. The expressions for the intensity of light in each mode have been published previously.⁶ The critical parameters are P_{core} and P_{clad} , which represent the amounts of power propagating in the core and cladding of each mode, re-

spectively. The intensity of the evanescent field calculated in these experiments is defined as the fraction of power propagating in the cladding, as shown in Eq. 1:

$$\eta_p = P_{\text{clad}} / (P_{\text{core}} + P_{\text{clad}}). \quad (1)$$

In this experiment we take advantage of the Beer's law relationship between the η_p and absorbance, which can be expressed as shown in Eq. 2:

$$A = \alpha \eta_p bc \quad (2)$$

where A is the absorbance, α is the absorption coefficient, b is the length of sensor, and c is the analyte concentration. The intensity of the evanescent field can be calculated by computing α from a transmission experiment, then solving for η_p , expressed in ppt (parts per thousand).

Length Considerations. One problem associated with optimizing evanescent field sensors is the relationship of absorbance to pathlength. Naively, one might estimate that it would be a linear relationship, as in the conventional Beer's law case. However, this is not even a good first approximation since, unlike the conventional case, each unit length of sensor will not provide the same absorption.

Consider a theoretical optical fiber which has two allowed modes of propagation: HE_{11} and HE_{21} . A V-number of approximately 3 is required to meet this criterion. The η_p for HE_{11} is approximately 10% and for HE_{21} it is approximately 35%. Assume that the analyte absorbs 100% of the light available in the cladding per unit length; the amount of light present in the cladding can be calculated as a function of position along the length of the sensor. Each unit length of sensor results in the absorption of all the available cladding energy, and a subsequent replenishing of the cladding with energy from the

TABLE I. Light distribution over a 10-cm sensor with two modes.^a

Position (cm)	HE_{11}		HE_{21}	
	W_{clad}	W_{core}	W_{clad}	W_{core}
0	0.02575	0.22420	0.08763	0.16238
1	0.02309	0.20111	0.05704	0.10533
2	0.02071	0.18040	0.03692	0.06841
3	0.01858	0.16180	0.02399	0.04445
4	0.01667	0.14510	0.01558	0.02887
5	0.01454	0.13020	0.01012	0.01875
6	0.01341	0.11680	0.00657	0.01218
7	0.01203	0.10480	0.00427	0.00791
8	0.01080	0.09400	0.00277	0.00514
9	0.00968	0.08430	0.00180	0.00334
10	0.00868	0.07560	0.00117	0.00217

^a W_{clad} is the light power in the cladding and W_{core} is the light power in the core.

Received 21 February 1992.

* Also Center for Laser Science and Engineering.

† Also Department of Physics, St. Ambrose University, Davenport, IA 52803.

‡ Department of Chemistry, Ohio University, Athens, OH 45701-2979.

§ Also Department of Physics and Astronomy. Author to whom correspondence should be sent.

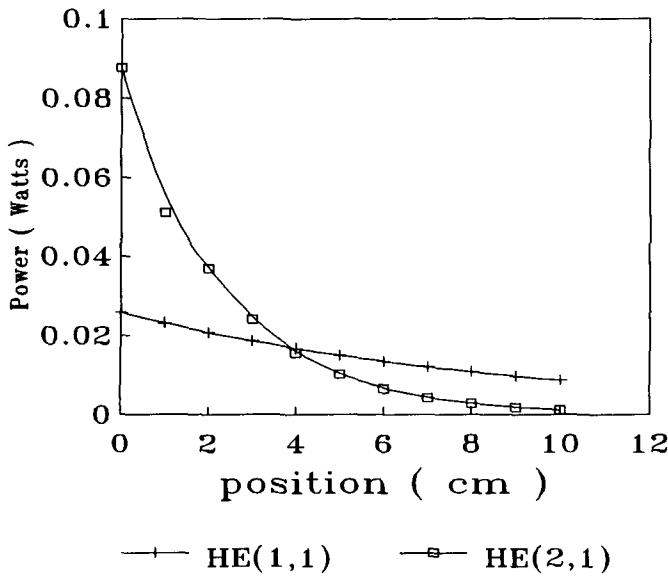


FIG. 1. Evanescent field intensity of HE_{11} and HE_{21} modes vs. position.

core. If we distribute 0.5 W of light evenly between two modes, the distribution of light over a 10-cm sensor would be as shown in Table I. This is illustrated graphically in Fig. 1, which shows the power in watts in the cladding of both modes. Note that the total η_p decreases with increasing position along the sensor; Fig. 2 shows the total η_p as a function of sensor position. The last centimeter of sensor is one-half as sensitive as the first centimeter. Repetition of this calculation on the mode distribution of the actual fiber to be used in the experiment results in the curve shown in Fig. 3. This effect is not significant in very long sensors since the evanescent field intensity reaches a stable value. In the generation of this curve, the absorption coefficient of water at the 5200 wavenumber band was used in place of a totally absorbing cladding. If the data in Fig. 3 are recalculated to give the total absorbance for the water band at a given sensor length and then compared to the conventional Beer's law pathlength relationship, the deviation becomes very apparent, as shown in Fig. 4.

Since throughput to the detector decreases with increasing sensor length due to increased scattering losses,

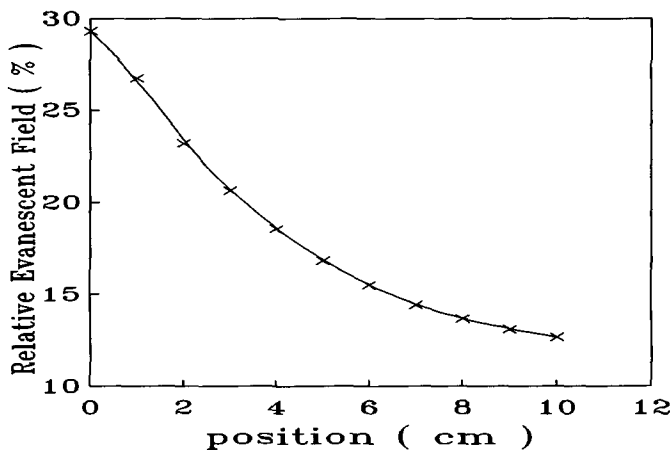


FIG. 2. Total evanescent field intensity vs. position.

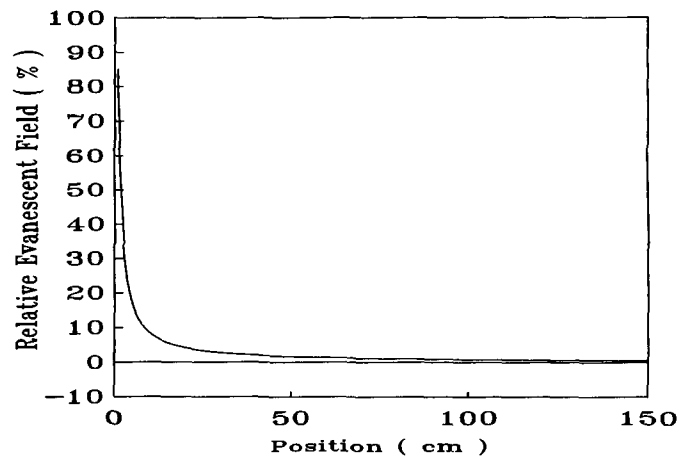


FIG. 3. Evanescent field intensity vs. position for a water analyte solution and a quartz sensor.

and the contribution of detector noise to a signal increases as the throughput decreases, these results suggest that there will be a sensor length which generates a maximum signal-to-noise ratio. The sensor length should be optimized as a part of the basic sensor design for a particular analyte.

Diameter Considerations. The second optimization problem is the sensor diameter. A simplified approach to the diameter effect on the evanescent field can be used to model the relationship between etching and evanescent field intensity for a given sensor. Consider the approximation of the η_p from the V -number as shown in Eq. 3:⁷

$$\eta_p \approx k/V. \quad (3)$$

The relationship between V -number and η_p is illustrated in Fig. 5. If all other fiber parameters are held constant, the relationship will reduce to Eq. 4:

$$\eta_p \approx k'/a \quad (4)$$

where k' is defined as shown in Eq. 5:

$$k' = k\lambda/(2\pi \cdot NA). \quad (5)$$

This indicates that the smaller the core radius, the larger the evanescent field; however, as in the length case,

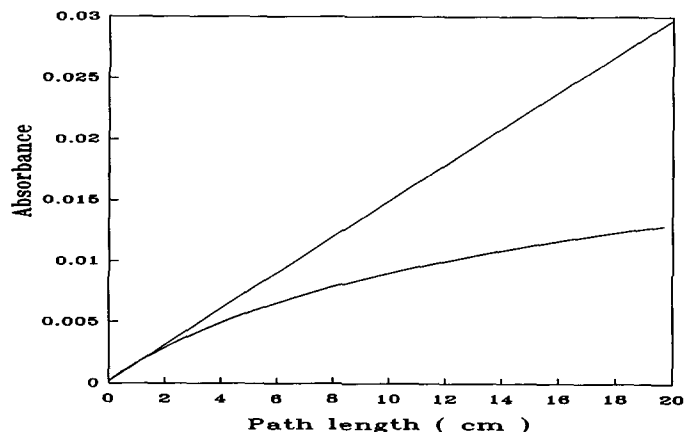


FIG. 4. Comparison of effective sensor pathlength (curved line) to Beer's law pathlength (straight line) for a quartz sensor.

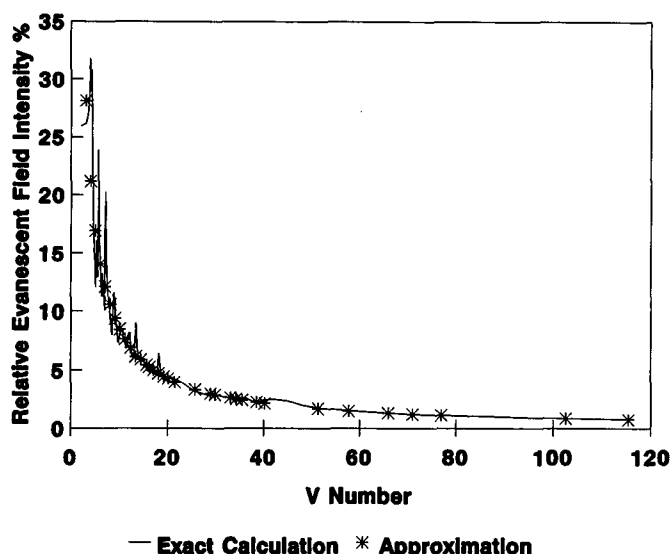


FIG. 5. Relative evanescent field intensity as a function of V -number.

throughput decreases with decreasing radius. The result should again be a diameter at which the signal-to-noise ratio goes through a maximum.

EXPERIMENTAL

The evanescent field sensors used in this work were constructed from 2-m lengths of Polymicro Technologies FIP 100-120-140 low-hydroxyl quartz optical fiber. The corresponding diameters of the core, cladding, and jacket were 100, 120, and 140 μm , respectively. The protective jacket was removed by refluxing in hot concentrated sulfuric acid for 10 min. This procedure exposes a clean surface for cladding removal.

The cladding of the fiber must be removed by etching with hydrofluoric acid. Initial experiments were performed with Newport FMLD fiber. This fiber is a silicon-silica fiber designed for general-purpose use. The ultraviolet and infrared ranges are limited, and viable

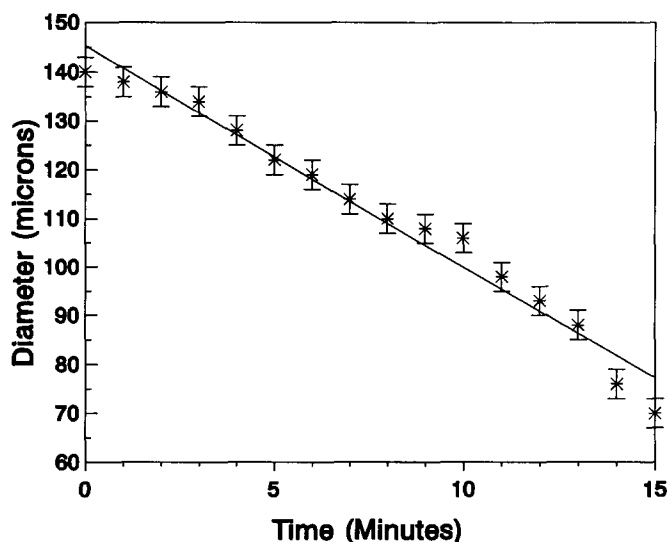


FIG. 6. Fiber diameter as a function of etch time. Newport FMLD fiber (core: 96 μm ; cladding: 140 μm), 48% hydrofluoric acid.

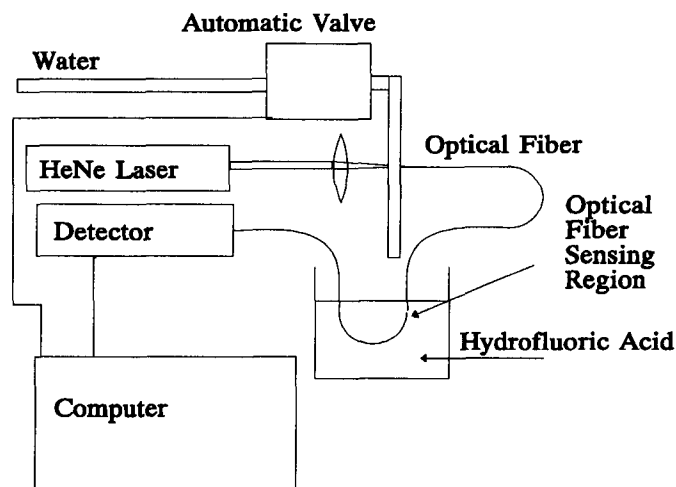


FIG. 7. Schematic of automatic etching system.

near-infrared sensors could not be constructed from this fiber. However, it is inexpensive, and allowed for perfection of the etching methodology prior to the use of more expensive quartz fibers.

The first experiment was to determine the relationship between etch time and diameter of the optical fiber. The Newport FMLD fiber (core: 96 μm , cladding: 140 μm) was stripped of its acrylic jacket over a 10-cm region with the use of methylene chloride. The fiber was immersed in a bath of 48% hydrofluoric acid for a period of time; it was then removed and the diameter measured with a micrometer. This procedure was repeated fifteen different times. The times ranged from 0 to 15 min. The measured diameter as a function of etch time is shown in Fig. 6. The relationship between diameter and etch time can be approximated by a linear relationship, which is adequate when reproducibility of a given etch is not required. However, in order to replicate sensor results, the reproducibility of the etching from sensor to sensor is a critical factor. Therefore, a more precise method of determining the diameter during the etching process was developed.

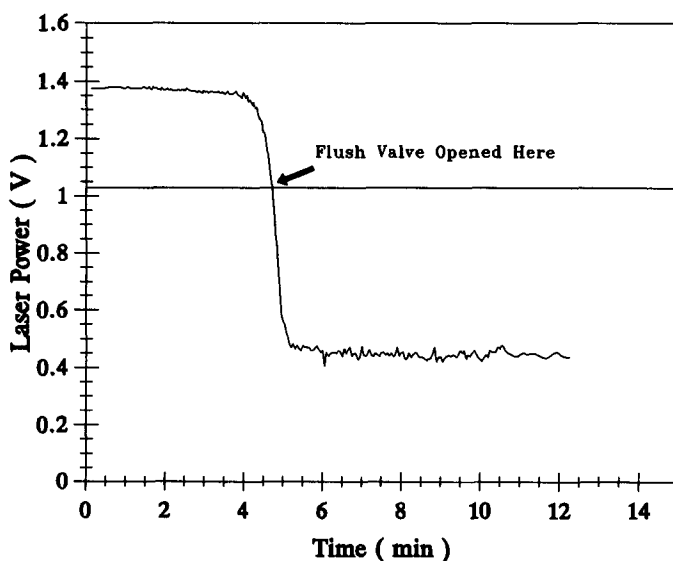


FIG. 8. Laser power vs. time: sensor etch profile.

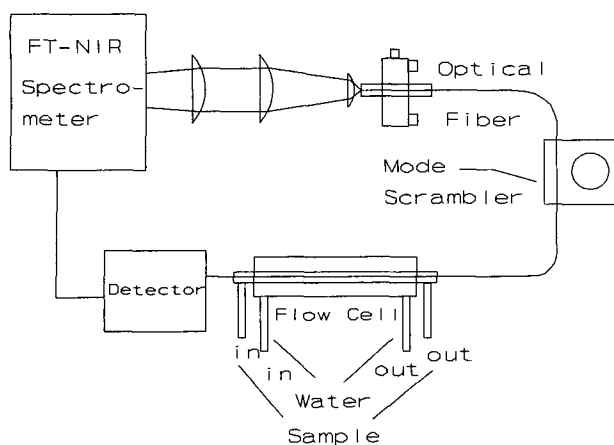


FIG. 9. Schematic representation of evanescent field sensor.

In an effort to improve the reproducibility of the etching procedure, a computer-controlled etching system was developed with the use of the decrease in signal from a helium neon laser as the monitor for etch depth. This system involves manually initiating the etching process by adding the hydrofluoric acid to a plastic vessel containing the optical fiber to be etched, without the protective jacket. When the acid is added, the computer is started, and the laser energy reaching the detector is monitored. When the energy level drops to a predetermined level, an automatic water valve is opened, and the vessel is flushed clean of hydrofluoric acid. This arrangement is shown schematically in Fig. 7. The data collection and automatic valve control were accomplished via a Strawberry Tree analog-to-digital (A/D) board. A TTL to 110 VAC conversion circuit was constructed to take the output of the A/D board and convert it to a signal the valve could use. The laser power profile obtained during a typical etch is shown in Fig. 8. The horizontal line in that figure represents the laser power threshold where the automatic valve was opened and the hydrofluoric acid rinsed from the fiber, halting the etching process. This procedure can provide diameter reproducibility within 5% provided that the length of the sensing region is held constant.

The experiments were carried out with a Nicolet 740

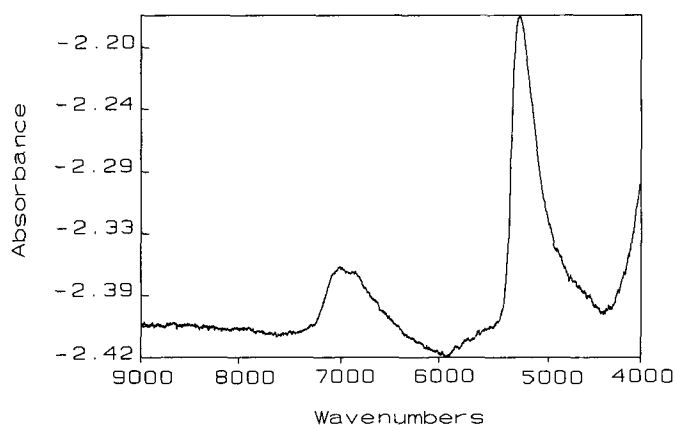


FIG. 10. Absorbance spectrum of water through an evanescent field fiber-optic sensor.

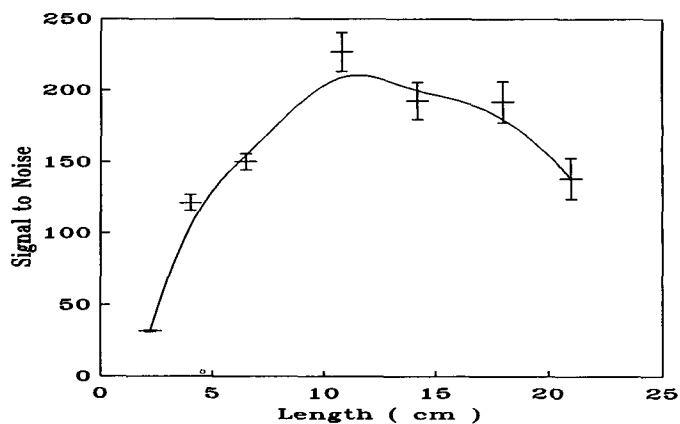
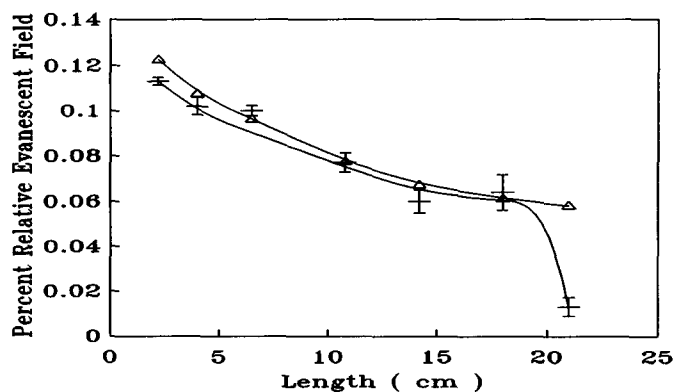


FIG. 11. Signal-to-noise ratio vs. sensor length calculated at 5200 cm^{-1} .

FT-IR instrument operating in the near-infrared with a CaF_2 beamsplitter, a tungsten-halogen source, and a cooled InSb detector. The completed sensor was mounted in a water-jacketed flow cell and interfaced to the spectrometer by the optical fiber interface illustrated in Fig. 9. The instrumental design is similar to that used by Degrandpre and Burgess,⁸ except that the fiber interface in this experiment occurs after the interferometer. The mode scrambling was accomplished with a Newport FM-1 mode scrambler. The absorbance spectrum of water and the total signal on the detector were recorded at a number of mode scrambler settings. A sample absorbance spectrum of water taken through the sensor is shown in Fig. 10. These spectra indicate that the spectra obtained from the evanescent field sensor are similar to those obtained with the use of transmission configurations. Sensor lengths from 2 to 21 cm were employed with the absorbance spectrum of water, and the total signal on the detector was recorded at each sensor length.

Experimentally, the effect of sensor diameter was tested with the same instrument design used in the sensor length study. In this case, the fiber sensor length was held constant and the diameter varied from 55 to 120 μm . It should be noted that, for diameters greater than 100 μm , cladding is still present on the sensor; this is a condition beyond the scope of the simple optical fiber



□ Experimental △ Calculated

FIG. 12. Evanescent field intensity vs. length; theoretical and experimental values.

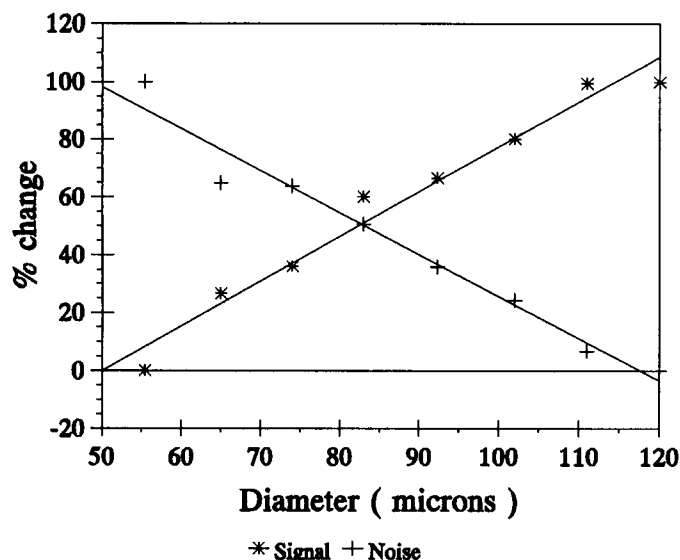


FIG. 13. Percentage change in absorbance and peak-to-peak voltage as a function of sensor diameter.

mode calculations, excluding them from ready comparison with theoretical values.

RESULTS

The absorbance of the water band at 5200 cm^{-1} was used to calculate the signal-to-noise ratio for each sensor length. Seven sensors ranging from 2.2 to 21 cm in length were tested, with three trials at each length. Figure 11 shows the signal-to-noise ratio plotted against sensor length. The error bars reflect the 95% confidence interval calculated from the standard deviation of the trials at each length.

If the η_p is back-calculated from the absorbance data and plotted against length (see Fig. 12), the data are very similar to the results obtained from the earlier calculations. The one extreme outlier is the 21-cm sensor. The deviation from theory for this data point is likely because the length becomes so long that all of the light is attenuated from the most evanescent modes, and subsequently the total evanescent field decreases much more rapidly. A second possibility is that the fiber was mechanically damaged during the etching process.

Due to problems associated with obtaining a reproducible etch when removing the cladding, conventional

signal-to-noise calculations did not result in an optimal diameter. The noise level was not reproducible from etch to etch, which caused the uncertainty associated with the signal-to-noise ratio to be very high. Therefore, an estimate of the noise was derived from the decrease in the detector peak-to-peak interferogram signal. This voltage should be inversely proportional to the noise. An alternative approach was employed to determine the optimal diameter for the sensor. The percent change in signal was plotted as a function of diameter on the same axis as was the percent change in the peak-to-peak voltage as a function of diameter (see Fig. 13). The point of intersection of these curves indicates the optimal sensor diameter. The optimal diameter in this case is approximately $82\text{ }\mu\text{m}$.

CONCLUSIONS

The combination of the decreasing evanescent field, the increasing signal due to the Beer's law pathlength relationship, and the decreasing throughput in the system results in the appearance of a maximum in the signal-to-noise ratio of an evanescent field fiber-optic sensor as a function of sensor length. The throughput and evanescent field intensity arguments cause the same to be true for sensor diameter. Therefore, it is necessary to optimize the sensor length and diameter experimentally for each analyte to produce the best sensor for a particular application. Ideally, the optimization should be done on both the length and diameter simultaneously to locate the global maximum in the signal-to-noise ratio for the particular application.

ACKNOWLEDGMENTS

We would like to thank the Iowa Corn Promotion Board and Cargill Inc. for funding this work.

1. N. Wright, R. Curbels, D. A. C. Compton, and S. L. Hill, *Infrared Fiber Optics*, SPIE **1048**, 153 (1989).
2. M. Degrandpre and L. Burgess, *Appl. Spectrosc.* **44**, 273 (1990).
3. C. Villarruel, D. D. Dominguez, and A. Dandridge, *Fiber Optic Sensors II*, SPIE **798**, 225 (1987).
4. F. Kvasnik and D. Mcgrath, *Chemical, Biochemical and Environmental Sensors*, SPIE **1172**, 75 (1989).
5. E. Snitzer, *J. Opt. Soc. Am.* **51**, 491 (1961).
6. T. Colin, K.-H. Yang, and W. Stwalley, *Appl. Spectrosc.* **45**, 1291 (1991).
7. P. Paul and G. Kychakoff, *Appl. Phys. Lett.* **51**, 12 (1987).
8. M. Degrandpre and L. Burgess, *Appl. Spectrosc.* **44**, 273 (1990).